Multiresponsive Dielectric Metasurfaces Based on Dual Light- and Temperature-Responsive Copolymers

Chengjun Zou, Purushottam Poudel, Sarah L. Walden, Katsuya Tanaka, Alexander Minovich, Thomas Pertsch, Felix H. Schacher,* and Isabelle Staude*

Tunability is essential for unlocking a range of practical applications of high-efficiency metasurface-based nanophotonic devices and systems. Increased research efforts in this area during recent years led to significant progress regarding tuning mechanisms, speed, and diverse active functionalities. However, so far almost all the demonstrated works are based on a single type of physical stimulus, thereby excluding important opportunities to enhance the modulation range of the metadevices, the available design options, as well as interaction channels between the metadevices and their environment. In this article, it is experimentally demonstrated that multi-responsive metasurfaces can be realized by combining asymmetric, highly resonant metasurfaces with multi-responsive polymeric materials. The respective copolymers combine light- and temperature-responsive comonomers in an optimized ratio. This work demonstrates clearly reversible light-responsive, temperature-responsive, and co-responsive tuning of the metasurface optical resonance positions at near-infrared wavelengths, featuring maximum spectral resonance shifts of nearly twice the full-width-at-half-maximum and accompanied by more than 60% absolute modulation in transmittance. This work provides new design freedom for multifunctional metadevices and can potentially be expanded to other types of copolymers as well. Furthermore, the studied hybrid multiresponsive systems are promising candidates for multi-dimensional sensing applications.

1. Introduction

Metasurfaces made of subwavelength resonators arranged in a plane have revolutionized the design options for optical components and system integration.[1] Various applications in imaging,[2,3] holography,[4,5] sensing,[6,7] and communication[8,9] were demonstrated within the past decade. Recently, inverse design methods[10,11] and metasurface-based diffractive deep neural networks[12,13] have further expanded the range of metasurface applications to areas such as optical signal processing[14–16] and all-optical computing.[17] Although tremendous research efforts were invested into metasurface-based applications, most of these static designs with "hard-coded" functions are still only significant in laboratory demonstrations rather than real-world applications. From a practical application perspective, realizing efficient tuning of the optical responses of metasurfaces is the key, which will ultimately unlock their full capabilities in arbitrary

C. Zou
Institute of Microelectronics
Chinese Academy of Sciences
Beitucheng west road 3, Beijing, China

C. Zou, S. L. Walden, K. Tanaka, A. Minovich, I. Staude
Institute of Solid State Physics
Friedrich Schiller University Jena
Max-Wien-Platz 1, 07743 Jena, Germany
E-mail: isabelle.staude@uni-jena.de

C. Zou, S. L. Walden, K. Tanaka, A. Minovich, T. Pertsch, I. Staude
Abbe Center of Photonics
Institute of Applied Physics
Friedrich Schiller University Jena
Albert-Einstein-Str. 15, 07745 Jena, Germany

P. Poudel, F. H. Schacher
Institute of Organic Chemistry and Macromolecular Chemistry
Friedrich Schiller University Jena
Lessing-Str. 8, 07743 Jena, Germany
E-mail: felix.schacher@uni-jena.de

P. Poudel, F. H. Schacher
Jena Centre for Soft Matter (JCSM)
Friedrich Schiller University Jena
Philosophenweg 7, 07743 Jena, Germany

P. Poudel, F. H. Schacher
Center for Energy and Environmental Chemistry (CEEC)
Friedrich Schiller University Jena
Philosophenweg 7, 07743 Jena, Germany

T. Pertsch
Fraunhofer Institute for Applied Optics and Precision Engineering
Albert-Einstein-Str. 7, 07745 Jena, Germany

wavefront shaping, programmable spatial light modulations, optical switching, and controlled emission processes.[18,19]

The realization of tunable metasurfaces requires the application of external physical stimuli to modify the resonance properties of the metasurface itself or its immediate surroundings.[19,20] Various tuning mechanisms have been demonstrated. For example, mechanical deformation[21,22] can lead to large tuning effects but usually with limited modulation speed. Carrier injection[23,24] and field effects,[25] in contrast, are fast and promising in high-speed modulations, though compromised by limited efficiency. Integrating phase-changing materials can be used for long-term reversible tuning.[26–28] Finally, integrating nematic liquid crystals (LCs) with metasurfaces has been widely studied,[29–32] motivated by the strong achievable tuning contrast, convenient electrical compatibility, and established LC-on-silicon technology. So far, however, with few exceptions,[33,34] the reported tunable metasurfaces are responsive to a single type of physical stimulus only. Multi-responsive tuning of metasurfaces, on the other hand, provides additional design options and allows for wider functionalities and interactions with the environment. In a previous work, we already reported a multiresponsive dielectric metasurface design via an integration with LCs and applying both thermal and electrical stimuli.[33] However, LCs are limited regarding the number of different stimuli and the possibility to tailor the respective responses. The integration of the metasurface with stimuli-responsive polymers[35,36] offers a general strategic advantage by means of multiple adjustable control parameters for achieving tunability. On the one hand, these polymers are capable of altering their chemical and/or physical properties upon exposure to external stimuli, for example, temperature, light, pH, or electric and magnetic fields.[37–43] On the other hand, different from plasmonic structures, the integration with dielectric metasurfaces can guarantee both high-efficiency and flexible capabilities of light manipulation.

Among the available triggers, temperature is the most applied and extensively investigated, with various studies exploiting the lower critical solution temperature (LCST) of different polymers.[37,44–47] The LCST is the temperature at which temperature-induced demixing occurs, hence, below the LCST the polymer chains are homogeneously dissolved, whereas above the LCST, phase separation happens through an entropically driven process. Some prevalent examples of such polymers include poly(N-isopropylacrylamide) (NIPAM),[46,48] poly(triethylene glycol acrylate) (TEGA),[44] poly(2-oxazolines)[49,50] and poly(oligo (ethylene glycol)acrylates).[51,52] Besides temperature, light has also attracted considerable attention as a versatile trigger in the field of stimuli-responsive polymers. Importantly, by using light of different wavelengths as a stimulus, the polymers can be controlled with high temporal and spatial precision. Light responsive materials can react reversibly by isomerization or irreversibly by photo-cleavage upon exposure to light. Among the different photo-responsive molecules, azobenzenes,[37,53] spiropyrans,[44,45] and diarylethenes[54] have been extensively investigated because of their high potential for applications such as data storage, light-switchable devices, optical sensors, or optical memory.[55,56] Furthermore, the combination of two or more stimuli-responsive materials allows the synthesis of multi-stimuli-responsive polymers. However, the selection

and preparation of the orthogonally addressable groups can be challenging. For example, dual light- and temperature-responsive copolymers can be synthesized by incorporating light-responsive comonomers into any temperature-responsive polymer. Such copolymers respond orthogonally to distinctly different stimuli through light-driven isomerization and temperature-driven phase separation.[37,40,44,45] Despite their rich chemistry and attractive properties, tunable hybrid systems that integrate dielectric metasurfaces with multi-stimuli-responsive polymers for high-efficiency optical applications, so far remain underexplored.

In this article, we propose and experimentally demonstrate multi-responsive tuning of dielectric metasurfaces via integration with multiresponsive polymer materials. The herein employed copolymers respond to both temperature and irradiation with light. Specifically, the light-responsive poly(azobenzene) (PAZO), temperature-responsive poly(triethylene glycol monomethyl methacrylate) (PTEGA), and dual light- and temperature-responsive P(TEGA-co-AZO) were synthesized using radical polymerization, respectively. This method also allows synthesis of many other types of polymers (e.g., responsive to pH, electric potential etc.) into one copolymer for tunable metasurfaces. Here we designed and fabricated metasurfaces consisting of geometrically asymmetric unit cells, which support several types of quasi-bound states in the continuum (quasi-BIC) modes[57,58] and other types of high-Q resonances[59] in the near-infrared wavelength range. By integrating the copolymer with the fabricated metasurface and applying light, temperature, or both as stimuli to the sample, clear reversible tuning of the resonance wavelengths could be observed. The maximum resonance shift reaches nearly two times of the full width at half maximum (FWHM) and features more than 60% absolute transmittance modulation. Our work opens new opportunities for the design of multifunctional metadevices. Furthermore, the demonstrated multi-dimensional interactions of the metasurface system with the surrounding environment is promising in applications such as ultrasensitive multivariable sensing.

2. Results and Discussion

2.1. Metasurface Design and Optical Characterizations

Figure 1a shows a sketch of a single unit cell of the designed metasurface. It consists of two rectangular silicon nanobars on a silica substrate. The unit cell is repeated in the x- and y-direction with the same period $p = 770$ nm. There are several symmetry breaks in the unit cell, which can lead to several quasi-BIC modes. The nanobars have slightly different designed lengths ($L_1 = 380$ nm and $L_2 = 350$ nm). The center-to-center distance of the nanobars is $g = 360$ nm, which is smaller than $p/2 = 385$ nm. The designed resonator height is $h = 280$ nm and the two nanobars also share the same width of $W_1 = W_2 = 200$ nm. Note that the design already considers a 500 nm P(TEGA-co-AZO) polymer coating layer, whose properties are discussed in the Supporting Information (SI) in detail. We fabricate the design with electron beam lithography (EBL) and inductively coupled plasma etching (see Experimental Section for details). During
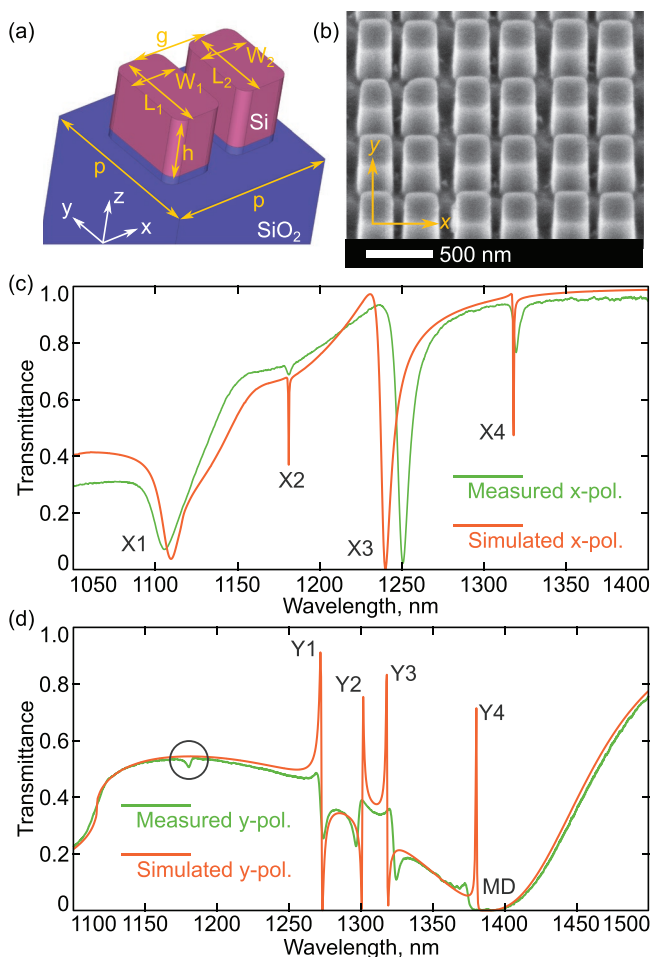
Figure 1. The metasurface and its transmittance spectra. a) Unit cell structure of the designed metasurface. b) Scanning electron micrograph of the fabricated metasurface, viewed at an azimuthal angle of 52°. c,d) Measured (green line) and calculated (orange line) transmittance spectra for the metasurface under c) x- and d) y-polarized normal incidence before the copolymer integration.

package CST Microwave Studio for a single unit cell with periodic boundary conditions. In order to optimize the agreement with the measured results, we obtained the metasurface size parameters from SEM and further optimized them within the limits of fabrication and measurement accuracy, yielding best agreement for $L_1 = 421$ nm; $W_1 = 245$ nm; $L_2 = 384$ nm; $W_2 = 248$ nm; $h = 273$ nm. The unit cell period $p = 770$ nm and center-to-center distance $g = 360$ nm were kept unchanged since they are usually accurately defined during fabrication. A shallow over-etch of 20 nm into the glass substrate observed in experiment was also included in the simulation. The calculated spectra are presented as red lines in Figure 1c,d, which capture all the measured features except the small dip at ≈1180 nm for the y-polarized results (marked by a black circle). In general, the y-polarized simulation shows a slightly better agreement with the measured spectrum than that for the x-polarization. The measured resonances are also less sharp than the simulated ones, which is likely caused by fabrication inaccuracies, such as surface roughness resulting in higher radiative losses. We label the main resonance features as X1 to X4 and Y1 to Y4 in Figure 1c,d, which are induced by the structural asymmetry. The near fields of these modes are presented and discussed in Section S1, Supporting Information. Moreover, by numerically varying the structural asymmetries, the quasi-BIC nature of these modes is studied in the Supporting Information, too.

2.2. Experiments for Light and Temperature Tuning

After examining the spectral features of the fabricated metasurface, we further investigate the metasurface integrated with stimuli-responsive polymers, aiming to tune the optical properties of the resulting hybrid systems by both light and temperature. Before doing this, the material properties of the stimuli-responsive polymers are discussed. The light-responsive PAZO, temperature-responsive PTEGA and dual light- and temperature-responsive P(TEGA-co-AZO) copolymers were synthesized by free-radical polymerization initiated with 2,2-azobis(isobutyronitrile) (AIBN). Further details regarding the copolymer synthesis can be found in Experimental Section. The polymers and copolymers were characterized by using a combination of size exclusion chromatography (SEC) and nuclear magnetic resonance spectroscopy (NMR), and their responses to both light and temperature were investigated using irradiation and/or heating by UV–vis spectroscopy. The SEC analysis of PAZO and PTEGA revealed a molar mass (M_n) of 6500 and 26 000 g mol^{-1} with rather broad dispersities (Đ) of 2.5 and 2.9, respectively (Table S1, Supporting Information). This fairly low M_n of PAZO for a free radical polymerization is in agreement with previously reported values.[60] Subsequently, a dual light- and temperature-responsive P(TEGA-co-AZO) was synthesized by copolymerization of TEGA with AZO using a feed ratio of 1:1 (**Figure 2**a). The copolymer ($M_n = 16\,000$ g mol^{-1} and Đ = 2.1) revealed the expected incorporation of both monomers and contained 36% AZO based on ^{1}H-NMR analysis (Figure S5, Supporting Information). It is known that PTEGA exhibits a lower critical solution temperature (LCST) at ≈ 57 °C which can be adjusted by varying the chain length and attaching hydrophilic or hydrophobic (end)groups.[44] The cloud-point

fabrication, eight EBL doses were adopted, resulting in a corresponding number of metasurfaces with varying feature sizes to be very different from the designed values. A scanning electron micrograph (SEM) image of the metasurface sample selected for tuning experiments is presented in Figure 1b.

First of all and before covering the silicon nanobars with the polymer coating layer, we characterized the optical transmittance of the fabricated metasurface in the near-infrared range using a customized setup (see Experimental Section). The measured spectra (green lines) are presented in Figure 1c,d for x-polarized and y-polarized light at normal incidence, respectively. For x-polarized incidence, two relatively broad resonance dips are observed at 1105 and 1251 nm. Two sharper but not so pronounced resonances occur at 1181 and 1319 nm. For y-polarized incidence, apart from a broad resonance at ≈1400 nm, several narrow dips were observed between 1250 to 1400 nm. To better understand the measured results, we performed full-wave numerical simulation of the metasurface transmittance spectra using the frequency-domain solver of the commercial software
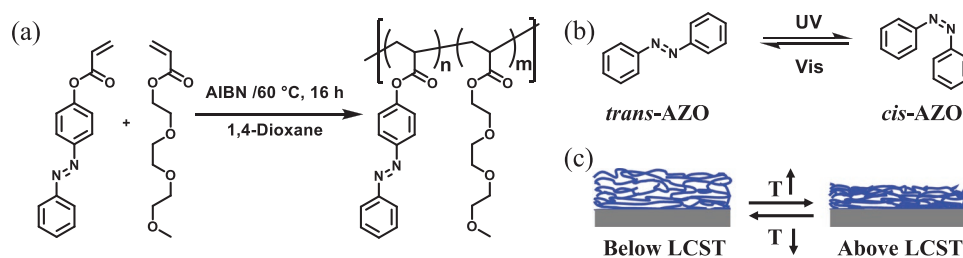
Figure 2. Copolymer synthesis. a) Synthesis of P(TEGA-*co*-AZO) in 1,4-dioxane by free radical copolymerization. b) *Trans-cis* isomers of the AZO side chain and photo-induced interconversion. c) Schematic diagrams show the thermoresponsive behavior of the PTEGA attached surface upon heating above or cooling below the LCST.

measurement of P(TEGA-*co*-AZO) revealed the reduction of the LCST from 57 to 30 °C as expected by the integration of the hydrophobic AZO- moiety in the copolymer (Figure S9, Supporting Information). To understand the light-response in general, a spin-coated copolymer film (on glass substrate) was characterized by UV–vis spectroscopy upon a UV (365 nm)/ visible light (450 nm) irradiation cycle (Figure S7, Supporting Information). The absorption spectrum of the as-prepared film exhibits the two characteristic bands: a high intensity $\pi \rightarrow \pi^*$ band in the UV region ($\lambda_{max} = 322$ nm) and a low-intensity $n \rightarrow \pi^*$ band in the visible region ($\lambda_{max} = 440$ nm). The UV irradiation at 365 nm leads to a gradual decrease in the absorbance at 322 nm and an increase in the intensity of the band at 440 nm. This indicates a transition from the *trans*- to the *cis*- form of the AZO-moiety. After 40 min of UV radiation (intensity details in Experimental Section), no further change was observed and a film preirradiated for 40 min with UV light was subsequently exposed to different times of visible light irradiation at 450 nm to switch back to the *trans*- form. When the visible light exposure reaches 20 min, the spectrum of the as-prepared film is fully recovered. In addition, a similar behavior was observed in tetrahydrofuran (THF) solutions (Figure S8, Supporting Information).

We would like to also briefly discuss the thermo-responsive behavior of polymers in solution and in solid thin films in general. In an aqueous solution, for a given polymer concentration, the thermo-responsive polymer coil is found in a highly hydrated, swollen, and hydrophilic state below the lower critical solution temperature (LCST). Heating above LCST results in a drastic increase in hydrophobicity and dehydration, facilitating a coil-to-globule transition. Unlike in solution, the solid thin film is not completely swollen with water since only the surface of the film is exposed to air, and the polymer chains are also constrained by the interfacial interactions. Several reports indicate that the temperature-responsive polymer film can absorb and store water from the air, thus causing swelling and a change in thickness with thermal treatment under atmospheric conditions.[61–63] This implies that when the temperature decreases below the LCST, water molecules can be adsorbed by the hydrophilic groups of P(TEGA-*co*-AZO) and the thin film partially swells. At the same time, the surface of the film is hydrophilic, whereas above LCST, a hydrophilic-to-hydrophobic transition occurs at the film surface.

Next, we spin-coated the synthesized polymers onto silicon substrates and characterized their optical refractive indices with ellipsometry for different material phases. Here, in situ

measurements with exposure to either UV (365 nm) or blue light (450 nm) and a feedback-controlled heating process were adopted (Figure S10, Supporting Information). In general, all the polymers show a decrease in their refractive indices with UV exposure or heating above their LCST, respectively. The changes in their refractive indices are in the order of 10^{-2}, which is expected to induce a resonance blueshift if coated onto our metasurface sample. When combining UV exposure and heating as co-stimuli, the P(AZO-*co*-TEGA) copolymer demonstrates a reduction of almost 0.04 in its refractive index. When illuminated by the blue light and allowed to cool down to room temperature (RT), the copolymer changes back to the initial phase with higher refractive index. Note that in the index fitting, the slight thickness variations were not considered and the resulting effects were included into the fitted data. The variations in polymer refractive indices observed here are small compared to those reported in other works (mainly electrochemically responsive polymers[64,65]). However, the material losses are also negligible for polymers used in this work, enabling high-efficiency optical applications.

After characterizing the refractive indices of the copolymers, we spin-coated PAZO, PTEGA, and P(TEGA-*co*-AZO) onto the fabricated sample and subsequently characterized the corresponding tunable transmittance. The resulting coating layers are expected to have thickness values of 400 to 500 nm according to the spin-coating recipe. First, we examined the tuning performance by integrating the sample with single-responsive polymers PAZO and PTEGA, respectively. For PAZO integration, UV light (365 nm; max. power 1290 mW; M365L3 Thorlabs) and blue light (450 nm; max. power 100 W) were employed as the stimuli. The UV light was located ≈13 cm from the sample and the light was collimated by a convex lens ($f = 20$ mm). The blue light broadly illuminated the sample without a focus. For PTEGA-integration, the temperature control was implemented using a 15 Ohm heating resistor and a PT100 RTD temperature sensor feedback system controlled via a temperature controller (LDT-5980, Newport) for high temperature (above critical temperature T_c) and RT control. The measured results are summarized in **Figure 3**, where three cycles of light-exposure/heating-cooling were adopted, showing that the respective tuning processes were reversible. More switching cycles were carried out for the case of copolymer integration, which are discussed in later sections. The obtained spectral resonance features look different from those of an uncoated metasurface, which is due to the optical properties of the coating layer. The structural asymmetry in the metasurface design
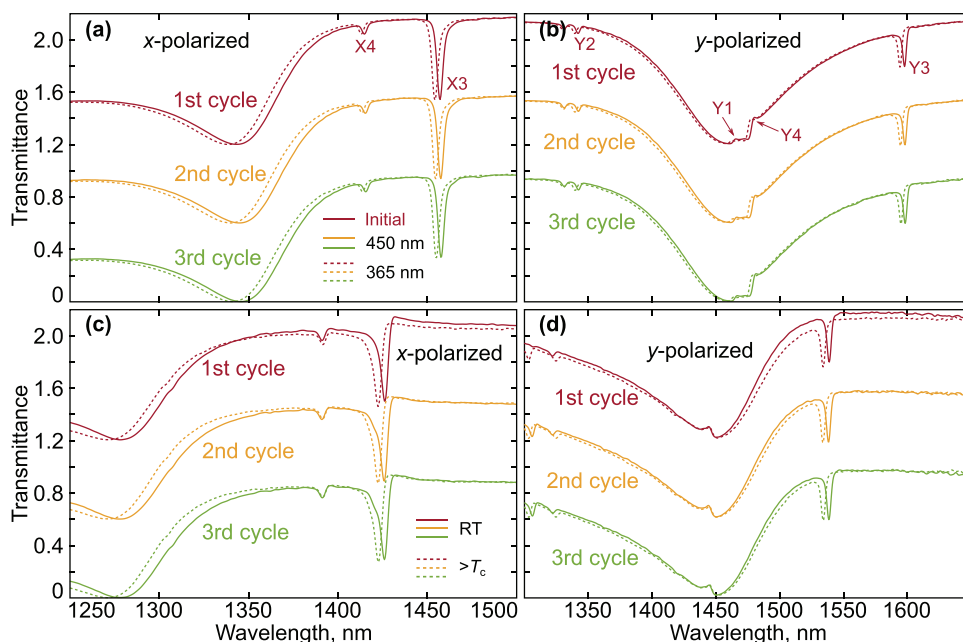
Figure 3. Cycled measurements for the metasurface integrated with a,b) the light-responsive polymer AZO and c,d) the temperature-responsive polymer TEGA under a,c) *x*- and b,d) *y*-polarized normal incidences. The results for the first and the second cycles are offset by 1.2 and 0.6, respectively, for clarity.

induces sharp resonances, which are highly sensitive to variation in the refractive index of the surrounding material (see Section S2, Supporting Information for a numerical study of the metasurface transmission spectra for a systematic variation of the refractive index of the coating layer). The observed resonance features of the coated metasurface shown in Figure 3 are labeled X3, X4 and Y1 to Y4, corresponding to the same modes for the uncoated metasurface. For PAZO coating, exposure to UV light causes the refractive index of the PAZO layer to decrease, leading to the resonance X3 to undergo a blueshift from 1458 to 1455 nm for *x*-polarization, nearly 50% of the resonance linewidth. The maximum transmittance modulation reaches 0.47 at 1454 nm. With blue light exposure, the dip shifts back to 1458 nm. Similar shifts were observed for the dip X4, and resonances Y1–Y3 for the *y*-polarization. For PTEGA integration, the modes X3 and X4, as well as Y3 occur at shorter wavelengths compared to these with PAZO coating, indicating a lower refractive index of PTEGA compared to PAZO. Upon heating of the sample beyond T_c of PTEGA, the dip X3 of the *x*-polarized incidence presented in Figure 3c, blueshifts from 1426 to 1423 nm, achieving a maximum transmittance modulation of 0.52. The dip recovers to the original position after cooling to RT. For *y*-polarization, the dip Y3 is less pronounced, but demonstrates a blueshift from 1538 to 1534 nm. The modes Y1 and Y4 merge in this case and cannot be distinguished. The results here clearly show that the phase-changing polymers can effectively tune the optical responses of metasurfaces. Also note that local heating effects from UV/blue light exposures are not observed during this work. The metasurface is not on resonance in the UV-blue range and the incident intensities are very low, leading to negligible local heating effects. Compared to other tunable metasurfaces integrated with electrically tunable polymers (such as PEDOT)[64,65] or phase changing materials (GST or VO₂),[26] the absolute spectral shifts in our work

are much smaller due to the comparatively small refractive index variations. However, different from the high material loss of PEDOT and GST, the material losses of PAZO and PTEGA are very small, and thus the transmittance modulation achieved here is higher. In addition, the high-Q quasi-BIC modes presented here can be well supported and tuned.

In the following, we focus on the multi-responsive properties of the metasurfaces integrated with the P(TEGA-*co*-AZO) copolymer. **Figure 4** summarizes the measured multi-responsive transmittance under *x*- and *y*-polarized incidence for the hybrid metasurface coated with the P(TEGA-*co*-AZO) copolymer. For the *x*-polarized results, the spectra in the range from 1250 to 1500 nm are presented, in which several main resonance features are observed. These resonance dips resemble the features observed with the single-responsive polymers, with an additional, weak dip ≈ 1465 nm that was not observed with single-responsive polymers. Small but distinct shifts can be seen in the resonance features following the application of different types of external stimuli. Here we mainly describe the shifts of the sharp resonance dip at ≈ 1450 nm. The black solid line represents the measured transmittance of the hybrid metasurface for the coated polymer in its initial phase at RT. Under these conditions, the minima of the sharp resonance are situated at 1451.6 nm. First we investigated the temperature-responsive behavior of the hybrid metasurface under the same conditions as that of the single-responsive tuning. For the P(TEGA-*co*-AZO) copolymer, a phase transition (TEGA-part) occurred at temperatures above the LCST (≈40 °C). The sample was heated to 45 °C (above T_c) and the corresponding transmittance was recorded and presented as the solid yellow line in Figure 4a. The sharp resonance blueshifts by 1 nm compared to the initial phase. Furthermore, when cooling the sample back to RT, the measured transmittance (dashed yellow line) shows a perfect overlap with the transmittance at the initial condition.
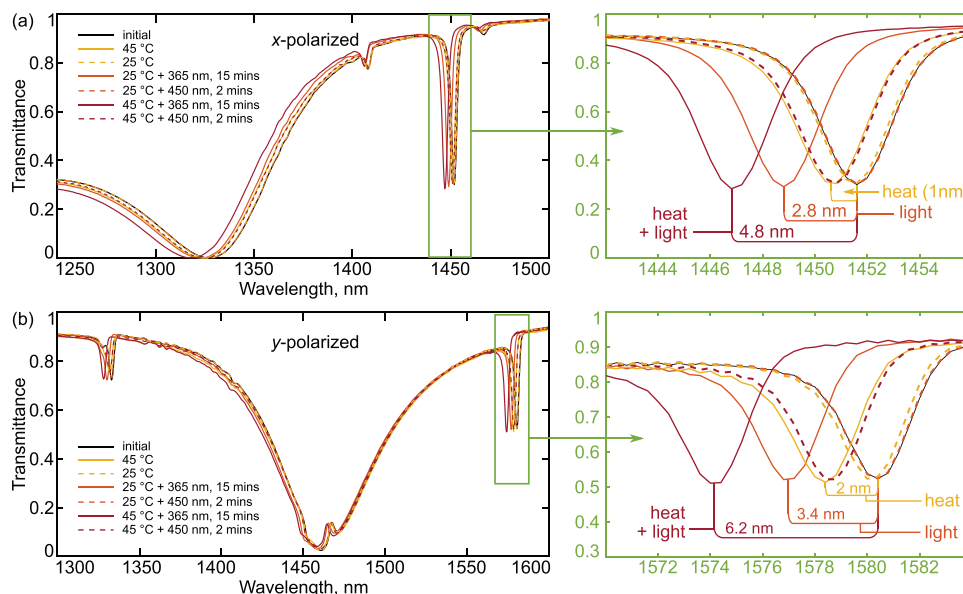
Figure 4. Experimentally measured transmission spectra of the metasurface covered with multi-response P(TEGA-*co*-AZO). Spectral shifts due to heat, UV light, and the dual application of heat and UV light are shown as solid lines, the spectra measured after the respective reverse stimuli (cooling, blue light) are shown as dashed lines.

Compared to the PTEGA-integration, the thermal-tuning range from the copolymer-integration is reduced, likely caused by the reduced TEGA portion, as well as smaller variations in the polymer layer thickness. Next, the sample was illuminated by UV light for 15 min. The light source was located 13 cm from the sample and was collimated by a lens with a focal length of 20 mm. After UV exposure, the sharp resonance (solid orange line) shifts to 1448.8 nm. Subsequent exposure to blue light for 2 min (450 nm, 100 W, located 15 cm away from the sample) produced a spectrum that overlaps with the transmittance of the hybrid metasurface in its initial state (orange dashed line), demonstrating the fully reversible, light-induced switching of the AZO units in the copolymer. Last but not the least, we investigate the light-temperature dual-responsiveness. For this, the sample was first illuminated with UV light for 15 min. When approaching such an illumination time, the sample was simultaneously heated to 45 °C. Both stimuli were then continuously applied while measuring the transmittance spectra. The result is represented by the dark red solid line in Figure 4a. Compared to the initial phase, application of both stimuli results in a blueshift of the sharp resonance of 4.8 nm to a final wavelength of 1446.8 nm, nearly twice of the FWHM. Interestingly, such a blueshift is wider than simply the combination of light-responsive (2.8 nm) and thermal-responsive (1 nm) stimuli only. The associated maximum absolute transmission modulation reaches 0.62 at 1451.6 nm. Although the resonance shifts in wavelengths are smaller compared to our previously reported multiresponsive metasurface[33] using LC integration, the absolute transmittance modulation is larger. We observed similar tuning effects for the broad resonance ≈1320 nm, as well as for the less pronounced resonant feature ≈1408 nm, however the corresponding transmission modulations and spectral shifts of these resonances are smaller compared to the dip ≈1450 nm. Additionally, we characterized the reverse tuning process by

illuminating the sample again with blue light for 2 min at 45 °C, the measured spectra (dark red dashed line) coincides with the yellow solid line, indicating that the fully reversible tuning of the AZO units is preserved at elevated temperatures.

For the *γ*-polarized results in Figure 4b, the measured spectra are shown in a range from 1300 to 1600 nm, which covers the respective resonance modes of interest. The right-hand-side of the plot shows a close-up of the spectral region around the sharp resonance feature between 1570 to 1584 nm. Altogether, a similar multi-responsive tuning behavior to that of the *x*-polarized case was obtained. The maximum blueshift of 6.2 nm from the initial state, observed for simultaneous application of both light and temperature as stimuli, is even larger than for *x*-polarization, reaching more than twice the FWHM of the resonance and realizing a high absolute transmission modulation well exceeding 0.4 at 1580 nm. For the broad resonance and less pronounced resonant features, similar tuning behavior was also observed.

2.3. Reversibility of the Stimuli-Response

After allowing the sample to cool to RT, we further evaluated the reversibility of the response of this hybrid system (**Figure 5**). First, five cycles of RT-T_c thermal tuning were performed and the results in Figure 5a show excellent reversibility of the resonance shifts. Subsequently, we continuously heat the sample with the temperature controller for 100 min, during which the sample temperature periodically oscillated between 32.6 to 44.4 °C. To implement the temperature variation, we made use of the temperature feedback control mechanism of the employed heater, which approaches a set target temperature in an oscillatory fashion. Note that as time progresses, the temperature variation is reduced to an interval from 35.5 to 40.5 °C as the system
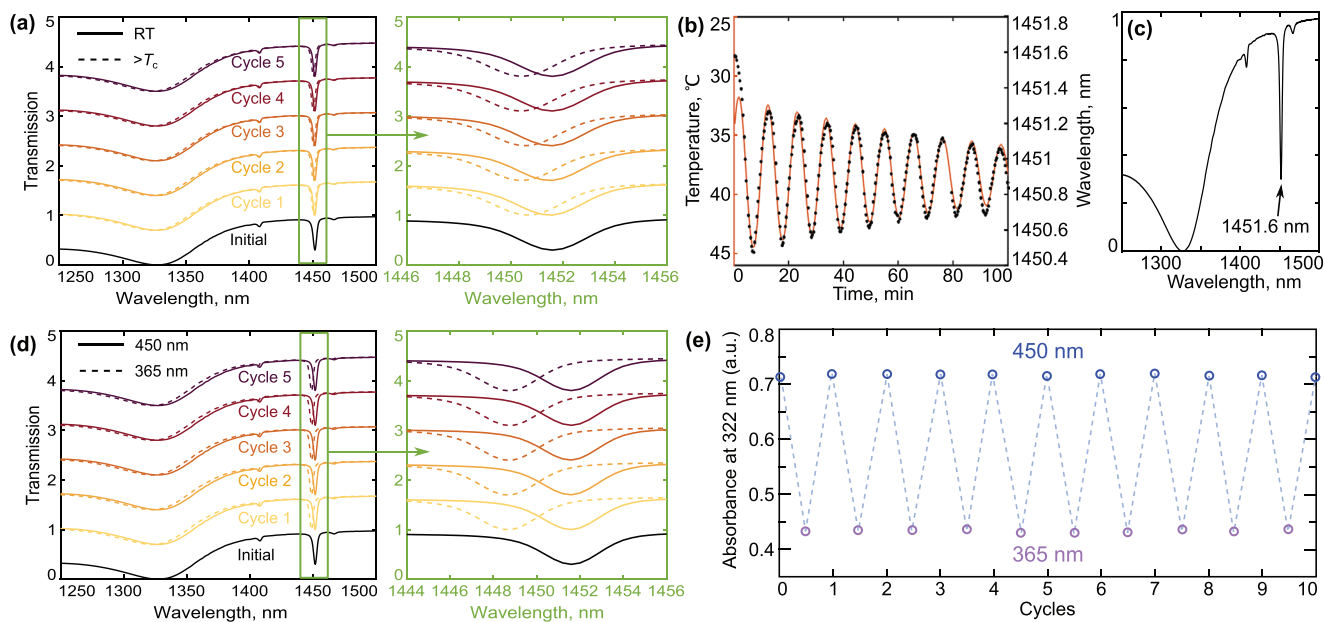
ADVANCED
SCIENCE NEWS
www.advancedsciencenews.com

ADVANCED
OPTICAL
MATERIALS
www.advopticalmat.de

Figure 5. Cycled temperature and light responsive tuning measurements on copolymer integrated metasurfaces. a) Five cycles of temperature tuning with full temperature range. b) Transmittance spectra of the sample at elevated temperature oscillated in between 32.6 to 44.4 °C. c) Measured transmittance spectrum of the sample recovered to RT. d) Transmittance spectra for cycled UV-blue light exposure. e) Absorbance characterization with UV–vis spectroscopy for cycled UV-blue light exposures.

moves closer to the set target temperature. The corresponding transmittance of the metasurface was recorded every 23 s and the results are shown in Figure 5b, which demonstrates periodic oscillation of the resonance wavelengths. Finally, the metasurface transmittance was characterized again after the sample cooled down to RT and the corresponding spectrum (Figure 5c) returns to the initial position, indicating long time reversibility of the TEGA units of the copolymer. As a next step, we carried out cycled light tuning measurements, where we also characterized the transmittance spectra with five cycles of UV-blue light exposure. In Figure 5d, the corresponding results demonstrate clearly that reversible spectral tuning of the resonance dip is possible. Afterward, the same sample underwent ten cycles where the corresponding absorbance was oscillated between low and high values, corresponding to the *cis*- and *trans*-state of the azobenzene units. From the whole set of data shown here, no obvious degradation of the copolymer material is visible.

2.4. Resonance Shift Kinetics

To fully characterize the light-responsive tuning speed, we record the resonance X3 shifting kinetics for UV and blue light exposure for the P(TEGA-*co*-AZO) coated metasurface. Please note that for these measurements the sample was freshly coated, which leads to slightly different resonance wavelengths due to a small variation in the coating layer thickness (**Figure 6**). The measured light intensities were 0.38 W cm^{-2} for the UV irradiation and 0.12 W cm^{-2} for the blue light. For UV exposure, the sharp resonance undergoes a hypochromic shift from λ_{min} = 1461.4 nm to λ_{min} = 1458.6 nm ($\Delta\lambda$ = 2.8 nm). It can be seen that 50% (1461.4 to 1460 nm) of the shift was achieved within the first 20 s. Similar kinetic features are seen for the blue light exposure. Therefore, it is expected that by increasing the illumination intensity, the switching speed can be largely accelerated.
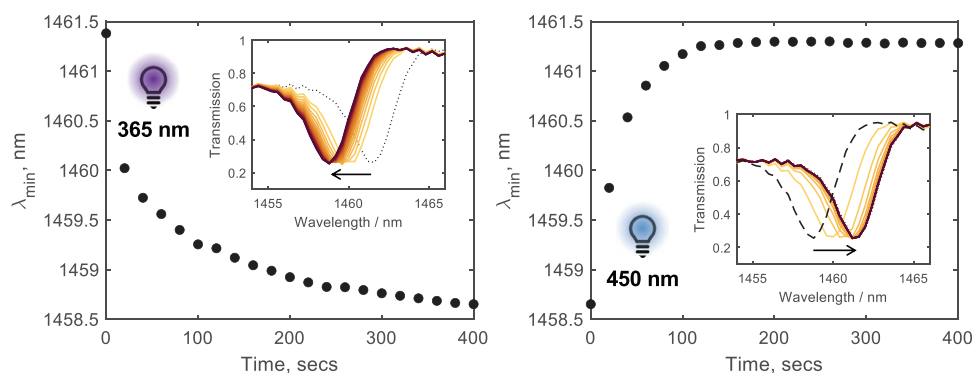

Figure 6. Kinetic tracking of the shift in the *x*-polarized transmission resonance at 1461.4 nm upon illumination with (left) 365 nm and (right) 450 nm light. Complete recovery of the initial peak position is obtained after 2 min of irradiation with blue light.
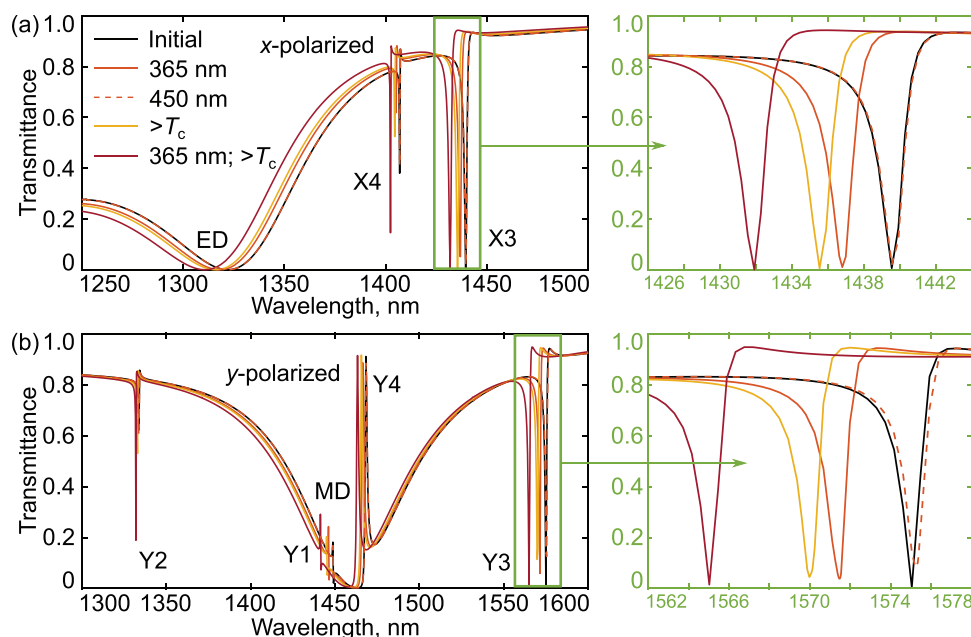
ADVANCED
SCIENCE NEWS
www.advancedsciencenews.com

ADVANCED
OPTICAL
MATERIALS
www.advopticalmat.de

Figure 7. Numerically calculated transmittance spectra of the hybrid metasurface assuming ellipsometrically determined optical properties for the multiresponsive copolymer P(TEGA-co-AZO) layer in its different states.

2.5. Discussion and Analysis

To further analyze the measured tuning results, we performed numerical simulations of the hybrid metasurfaces, assuming a coated copolymer layer of 500 nm on the metasurface. We modeled the coating layer with the ellipsometrically determined refractive indices for the corresponding phase states of the multi-responsive polymer. Here, only the case of copolymer integration is numerically studied, and the resonance modes are the same for PAZO and PTEGA integrations. The simulated layer thickness was taken to be 500 nm. We did not fit the layer thickness since varying it only spectrally shifts the wavelengths of the observed dips. When the coating layer exceeds 600 nm, no further shift in the simulated spectra is observed.

Figure 7 presents the simulated transmittance spectra of the integrated metasurface. Qualitatively, the simulated spectra are in excellent agreement with the experimental data (see Figure 4) regarding the resonance structure of the metasurface sample. A general blueshift of all resonance positions is observed with respect to experimental data, likely due to discrepancies in the characterized copolymer refractive indices and coated layer thickness. To identify the nature of the different resonances, we furthermore study the near-field profiles at the corresponding resonance wavelengths and present them in **Figure 8**. For the x-polarization, three main resonances are observed in the wavelength range of interest. The broad resonance ≈1310 nm is identified as an electric dipole (ED) resonance. The other two sharp resonances initially located ≈1407 and 1440 nm, and labeled as X4 and X3, respectively, are the same modes as labeled in Figure 1c. It can be seen that X4 is an in-plane antiferromagnetic (AFM) order with an out-of-plane ED moment induced in-between the two nanobars. X3 is an out-of-phase coupled out-of-plane ED pair, which induces a magnetic dipole (MD) moment between the two bars. Note that here the highest

E-fields occur in the shallow glass pedestal marked by the blue ellipse, caused by over-etching into the silicon layer during fabrication, while the field intensity is lower in the resonators. When applying the refractive index measured for the polymer after UV exposure to the coating layer in the simulations, the resonance positions shift to 1405 and 1437 nm (Figure 7, orange line). Blue light exposure brings them back to the initial position (Figure 7, orange dashed line). Next, when assigning the coating layer the refractive index for the case of heating above the critical temperature, the two resonances shift to 1404.5 and 1435.5 nm (Figure 7, yellow line). Finally, with the refractive index of the coating layer set to the values measured for simultaneous application of both stimuli, the two resonances shift to 1402.5 and 1432 nm (Figure 7, dark red line). Overall, we can conclude that the resonance shifts obtained by the model are consistent with experimental demonstrations. For the y-polarized results, the simulation also qualitatively captures all the essential measured features. Again, by conducting an analysis of near-field profiles of the relevant modes (Figure 8), we can identify the relatively broad resonance at 1455 nm as a MD mode and labeled other sharp features as Y1 to Y4, which are in consistent with modes denoted in Figure 1d. The near-field profiles of Y1 to Y4 are also displayed in Figure 8. We briefly describe the resonances from short to long wavelengths. First of all, Y2 corresponds to an out-of-phase coupled pair of in-plane MDs. Y1 and Y4 are identified to be the out-of-plane MDs mainly supported by the bigger and smaller nanobars, respectively. Y3 represents an out-of-plane MD resonance, created by the in-plane ED moment asymmetry in the two bars. The maximum enhancements for these resonances are all astonishingly high, which results from two factors: first, the small asymmetry in the two bar lengths and interbar distance; and second, the additional confinement mediated by the coating layer. However, the averaged enhancements in the metasurface volume are much lower.
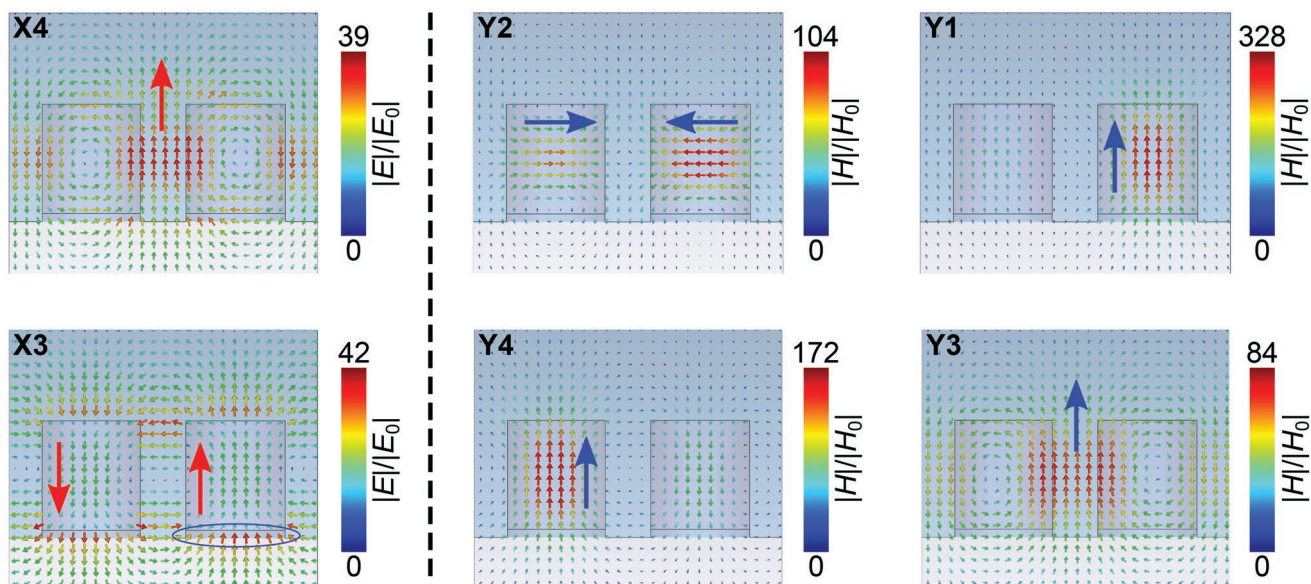
Figure 8. Numerically calculated near-field profiles at the center of the two nanobars on the *x*–*z* plane for the sharp resonance features marked in Figure 7. Red and blue arrows are used to denote the electric and magnetic moments.

The resonance shifts are larger in simulation than that in the measured results. Particularly, the temperature-responsive resonance shifts (Figure 7, yellow lines) are significant in simulation, even larger than the simulated light-responsive shifts (Figure 7, orange lines), contrary to the experimental results. We infer that possible inaccuracy in the refractive indices of the copolymer exists and leads to the results. As the slight thickness variations due to the TEGA units were not considered in the ellipsometry, it is likely the obtained index variations were overestimated and thus results in a larger thermal-responsive blueshift in simulation. Moreover, the maximum transmittance modulation is over 90% in the simulations, due to the larger resonance shifts and higher resonance *Q*-factors compared with the measurements. This is expected since the simulation model did not include the possible large parameter asymmetries, shape roughness, as well as a possible nonuniform coating layer in the fabricated sample, which can largely increase the radiative losses and decrease the *Q*-factors. To achieve larger transmittance modulation and resonance shifts, different polymer materials or synthesized copolymers can be used. The metasurface design and the polymer integration process can also be further optimized.

3. Conclusion

In conclusion, we demonstrated that hybridization of a metasurface with a multi-responsive copolymer allows tuning of the metasurface resonance frequencies using light, temperature, or a combination of both as external stimuli. Specifically, we spin-coated an asymmetric silicon metasurface supporting high-*Q* resonances, including quasi-BIC modes, with a multi-responsive P(TEGA-*co*-AZO) copolymer. By applying either UV exposure or a thermal stimulus only to the hybrid metasurface, small resonance blueshifts were observed, which were

in good agreement with results from accompanying numerical simulations. By simultaneously applying both the UV exposure and heating over the critical temperature for the temperature-triggered phase transition of PTEGA, an even larger resonance shift could be observed, reaching almost twice the FWHM of the resonance. This shift is accompanied by an absolute transmission modulation exceeding 0.6. Furthermore, we demonstrated the full reversibility of the tuning by performing more than ten cycles of switching experiments for integration of the metasurface with the copolymer, and no obvious degradation is observed. Our work opens a new access route toward multi-responsive metasurfaces and devices, which are promising for metasystems that can adapt to a complex environment as well as for highly compact multi-dimensional sensing applications.

4. Experimental Section

Metasurface Fabrication: For the fabrication of the silicon metasurfaces, standard electron beam lithography was performed in combination with reactive ion etching. As a first step, amorphous silicon thin films situated on a glass substrate (Tafelmaier Dünnschicht Technik GmbH) were etched by argon-ion beam etching to the target silicon thickness (270 to 280 nm) and covered with a conductive chromium layer. After that, a negative electron-beam resist (100 nm EN038, Tokyo Ohka Kogyo Co., Ltd.) was spin-coated onto the sample, exposed by a variable-shaped electron-beam lithography system (Vistec SB 350), and selectively dissolved in a developer (OPD 4262). After transferring the exposed pattern to the chromium layer by ion-beam etching (Oxford Ionfab 300), the silicon layer was etched through the chromium mask by reactive ion etching (RIE-ICP, Sen-tech SI-500 C). As a final step, the remaining resist and the chromium mask were removed in acetone and ceric ammonium nitrate-based solution, respectively.

Transmittance Measurements: The transmittance spectra of the metasurfaces were characterized with a custom-built optical setup as shown in **Figure 9**. A halogen lamp was used as the white light source, with the condenser lens collimating its emission. The diaphragm plane was in conjugation with the sample plane and was used to define the
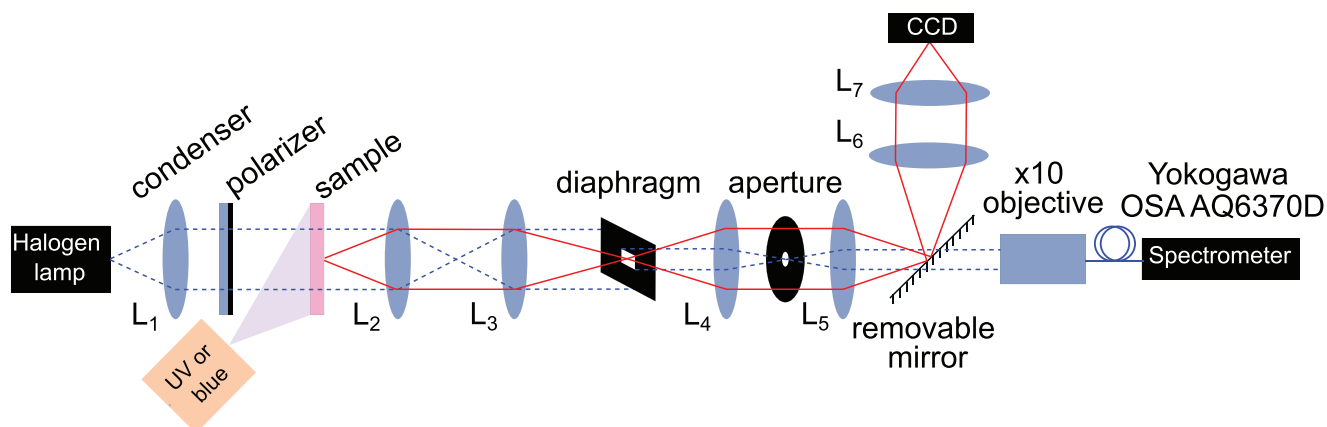
**ADVANCED
SCIENCE NEWS**

www.advancedsciencenews.com

**ADVANCED
OPTICAL
MATERIALS**

www.advopticalmat.de

Figure 9. Optical setup for transmittance measurements under UV/blue light exposure. The focal lengths of the marked lenses L_1 to L_7 are: 7, 50, 100, 50, 50, 50, and 200 mm.

measurement area. An aperture in the Fourier plane was used to limit the spread of incidence angles and ensure near normal incidence (within ±1°). The two optical paths denoted by the dashed blue and red lines denote the transmittance measurement path and the sample imaging path, respectively. The removable mirror was used for selecting the imaging path (for sample alignment) or the actual measurement path. Finally, a Yokogawa AQ6370D optical spectrum analyzer was employed to record the spectra at near infrared wavelengths. For light-responsive tuning experiments, the illuminating LEDs (blue or UV) were positioned aside without focusing.

Polymer Synthesis and Characterization—Chemicals: 4-Phenylazophenol, acryloyl chloride (97.0%), and 2, 2-Azobis(isobutyronitrile) (AIBN) were purchased from Sigma-Aldrich (Munich, Germany). AIBN was purified by recrystallization from ethanol and stored in the freezer until use. Triethylene glycol acrylate (TEGA 97%) were purchased from TCI (Zwijndrecht, Belgium) and purified using either inhibitor remover (Sigma-Aldrich) or by passing through a short aluminum oxide column. All other reagents were used as received.

NMR measurements were carried out on a 300 MHz Bruker NMR spectrometer (Karlsruhe, Germany) $CDCl_3$ or CD_2Cl_2 at 298 K. Chemical shifts are given in parts per million (ppm, δ scale) relative to the residual signal of the deuterated solvents.

SEC measurements were performed on a Shimadzu system equipped with an SCL-10A system controller, an LC-10AD pump, and a RID-10A refractive index detector using a solvent mixture containing chloroform ($CHCl_3$), triethylamine (TEA), and isopropanol (i-PrOH) (94:4:2) at a flow rate of 1 mL min^{-1} on a PSS SDV linear M 5 µm column. The system was calibrated using PS (100 to 100 000 g mol^{-1}) and PEO (440 to 44 700 g mol^{-1}) standards.

UV–vis measurements were performed on an Agilent (Santa Clara, CA, USA) Cary 60 UV–vis spectrometer with a peltier single cell holder. For the solid-state UV–vis measurements, the solid samples (deposited on glass substrates) were placed on a custom-made sample holder. Irradiation sources, two LEDs with 365 nm (0.8 mW) and two LEDs with 450 nm (22 cd) from Roithner (Vienna, Austria) were placed in front of the sample, resulting in an estimated light intensity of 3.4 mW cm^{-2} for the 365 nm light source, and 4.5 mW cm^{-2} for the 450 nm LED in the setup used. For the cloud point temperature measurements, the samples were placed in quartz cuvettes and heated from 20 to 70 °C at a rate of 1 °C min^{-1} without stirring. Cloud points were determined at $\lambda = 600$ nm and 50% transmittance. The transition window (ΔT) corresponds to the 1% and 99% transmittance temperature difference.

Thin-Film Preparation: The synthesized homopolymers and copolymers were dissolved in tetrahydrofuran at 100 °C to form the solutions of 2.5–5 wt% and filtered with a polytetrafluoroethylene (PTFE) syringe filter of pore size of ≈0.22 µm. These solutions were subsequently used for the spin coating to form the films of thicknesses

(h) ranging from 150 to 450 nm on freshly piranha cleaned silicon substrates. All the films were spin-coated at a constant rotation speed of 1500 rotations per minute for 5 min.[66] The thicknesses of the resulting polymer films were determined via atomic force microscopy. *Synthesis of 4-Phenylazophenyl Acrylate*: 4-Phenylazophenyl acrylate (AZO) was synthesized as described elsewhere.[67] Briefly, 4-hydroxyazobenzene (0.2 mol) and triethylamine (0.26 mol) were dissolved in diethyl ether (200 mL). The solution was purged with nitrogen and cooled to 0 °C. To this solution, acryloyl chloride (0.24 mol) dissolved in 80 mL of diethyl ether was added dropwise with stirring. The reaction mixture was allowed to come to room temperature and stirred for 8 h. The reaction solution was filtered to remove triethylammonium salt, washed with water, and evaporated. The product was recrystallized twice from the ethanol-water (3:1) mixture and dried in vacuo. The structure was confirmed by ^1H-NMR (Bruker, 300 MHz, $CDCl_3$). δ (ppm) = 6.0–6.9 (m, 3H), 7.3–7.7(m, 5H), 7.8–8.1 (m, 4H)

Synthesis of PAZO and PTEGA Homopolymers: PAZO and PTEGA were synthesized as follows: 1.0 g of AZO (or TEGA) was dissolved in 5 mL 1,4-dioxane. Then 50 mg (5 wt %, 3.04×10^{-4} mol) of 2,2-azobisisobutyronitrile (AIBN) was added, and the mixture was heated at 70 °C for 18 h under argon. The reaction mixture of PAZO was then precipitated three times in cold hexane and dried at 70 °C for 24 h. In the case of PTEGA, the reaction mixture was dialyzed against water and freeze-dried to form a colorless oil. The resulting polymers were analyzed via SEC and ^1H-NMR.

PAZO: ^1H-NMR (300 MHz, CD_2Cl_2): $\delta = 8.0$–7.0 (Ar–H) and SEC ($CHCl_3$): $M_n = 6500$ g mol^{-1}, and PDI = 2.5. PTEGA: ^1H-NMR (300 MHz, $CDCl_3$): $\delta = 3.3$ (s, 3H, CH_3, TEGA) and SEC ($CHCl_3$): $M_n = 26\,000$ g mol^{-1}, and PDI = 2.9.

Synthesis of Dual Light- and Temperature-Responsive P(TEGA-co-AZO): The copolymers containing light-responsive AZO and temperature-responsive TEGA (1:1 molar ratio) were synthesized through free radical polymerization as follows: TEGA (332 mg, 1.52 mmol), AZO (384 mg. 1.52 mmol), and AIBN (5 mg, 0.03 mmol) was dissolved in 1, 4-dioxane (5 mL). The mixture was deoxygenated by flushing with argon for 30 min and then heated in a sealed microwave vial to 70 °C for 18 h. The reaction mixture was then precipitated three times in cold diethyl ether. Finally, the product was dried under a vacuum and a yield of 51% was obtained. The copolymers were analyzed by SEC and 1H-NMR.

1H-NMR (300 MHz, CD_2Cl_2): $\delta = 3.3$ (s, 3H, CH_3, TEGA), and 7.8 (s, 4H, CH, Ar–H) ppm.

SEC ($CHCl_3$): $M_n = 16\,000$ g mol^{-1}, and PDI = 2.1.

Supporting Information

Supporting Information is available from the Wiley Online Library or from the author.

[1] W. T. Chen, F. Capasso, *Appl. Phys. Lett.* **2021**, *118*, 100503.

[2] Z. Li, P. Lin, Y.-W. Huang, J.-S. Park, W. T. Chen, Z. Shi, C.-W. Qiu, J.-X. Cheng, F. Capasso, *Sci. Adv.* **2021**, *7*, eabe4458.

[3] S. Banerji, M. Meem, A. Majumder, F. G. Vasquez, B. Sensale-Rodriguez, R. Menon, *Optica* **2019**, *6*, 805.

[4] Q. Song, X. Liu, C.-W. Qiu, P. Genevet, *Appl. Phys. Rev.* **2022**, *9*, 011311.

[5] E. Arbabi, S. M. Kamali, A. Arbabi, A. Faraon, *ACS Photonics* **2019**, *6*, 2712.

[6] M. L. Tseng, Y. Jahani, A. Leitis, H. Altug, *ACS Photonics* **2020**, *8*, 47.

[7] I. Kim, W.-S. Kim, K. Kim, M. A. Ansari, M. Q. Mehmood, T. Badloe, Y. Kim, J. Gwak, H. Lee, Y.-K. Kim, *Sci. Adv.* **2021**, *7*, eabe9943.

[8] L. Zhang, M. Z. Chen, W. Tang, J. Y. Dai, L. Miao, X. Y. Zhou, S. Jin, Q. Cheng, T. J. Cui, *Nat. Electron.* **2021**, *4*, 218.

[9] L. Zhang, X. Q. Chen, S. Liu, Q. Zhang, J. Zhao, J. Y. Dai, G. D. Bai, X. Wan, Q. Cheng, G. Castaldi, *Nat. Commun.* **2018**, *9*, 4334.

[10] Z. Li, R. Pestourie, J.-S. Park, Y.-W. Huang, S. G. Johnson, F. Capasso, *Nat. Commun.* **2022**, *13*, 2409.

[11] R. Zhu, T. Qiu, J. Wang, S. Sui, C. Hao, T. Liu, Y. Li, M. Feng, A. Zhang, C.-W. Qiu, *Nat. Commun.* **2021**, *12*, 2974.

[12] J. Li, D. Mengu, N. T. Yardimci, Y. Luo, X. Li, M. Veli, Y. Rivenson, M. Jarrahi, A. Ozcan, *Sci. Adv.* **2021**, *7*, eabd7690.

[13] Z. Wang, L. Chang, F. Wang, T. Li, T. Gu, *Nat. Commun.* **2022**, *13*, 2131.

[14] H. Rajabalipanah, A. Abdolali, S. Iqbal, L. Zhang, T. J. Cui, *Nanophotonics* **2021**, *10*, 1753.

[15] H. Kwon, D. Sounas, A. Cordaro, A. Polman, A. Alù, *Phys. Rev. Lett.* **2018**, *121*, 173004.

[16] J. Zhou, S. Liu, H. Qian, Y. Li, H. Luo, S. Wen, Z. Zhou, G. Guo, B. Shi, Z. Liu, *Sci. Adv.* **2020**, *6*, eabc4385.

[17] L. Li, H. Zhao, C. Liu, L. Li, T. J. Cui, *eLight* **2022**, *2*, 7.

[18] J. Kim, J. Seong, Y. Yang, S.-W. Moon, T. Badloe, J. Rho, *Adv. Photonics* **2022**, *4*, 024001.

[19] T. Badloe, J. Lee, J. Seong, J. Rho, *Adv. Photonics Res.* **2021**, *2*, 2000205.

[20] C. Zou, J. Sautter, F. Setzpfandt, I. Staude, *J. Phys. D: Appl. Phys.* **2019**, *52*, 373002.

[21] P. Gutruf, C. Zou, W. Withayachumnankul, M. Bhaskaran, S. Sriram, C. Fumeaux, *ACS Nano* **2016**, *10*, 133.

[22] A. She, S. Zhang, S. Shian, D. R. Clarke, F. Capasso, *Sci. Adv.* **2018**, *4*, eaap9957.

[23] M. R. Shcherbakov, S. Liu, V. V. Zubyuk, A. Vaskin, P. P. Vabishchevich, G. Keeler, T. Pertsch, T. V. Dolgova, I. Staude, I. Brener, *Nat. Commun.* **2017**, *8*, 17.

[24] S. Makarov, S. Kudryashov, I. Mukhin, A. Mozharov, V. Milichko, A. Krasnok, P. Belov, *Nano Lett.* **2015**, *15*, 6187.

[25] P. Thureja, G. K. Shirmanesh, K. T. Fountaine, R. Sokhoyan, M. Grajower, H. A. Atwater, *ACS Nano* **2020**, *14*, 15042.

[26] A. Leitis, A. Heßler, S. Wahl, M. Wuttig, T. Taubner, A. Tittl, H. Altug, *Adv. Funct. Mater.* **2020**, *30*, 1910259.

[27] A. Howes, Z. Zhu, D. Curie, J. R. Avila, V. D. Wheeler, R. F. Haglund, J. G. Valentine, *Nano Lett.* **2020**, *20*, 4638.

[28] A. Howes, W. Wang, I. Kravchenko, J. Valentine, *Optica* **2018**, *5*, 787.

[29] A. Komar, Z. Fang, J. Bohn, J. Sautter, M. Decker, A. Miroshnichenko, T. Pertsch, I. Brener, Y. S. Kivshar, I. Staude, *Appl. Phys. Lett.* **2017**, *110*, 071109.

[30] S.-Q. Li, X. Xu, R. M. Veetil, V. Valuckas, R. Paniagua-Domínguez, A. I. Kuznetsov, *Science* **2019**, *364*, 1087.

[31] P. Yu, J. Li, N. Liu, *Nano Lett.* **2021**, *21*, 6690.

[32] C. Zou, A. Komar, S. Fasold, J. Bohn, A. A. Muravsky, A. A. Murauski, T. Pertsch, D. N. Neshev, I. Staude, *ACS Photonics* **2019**, *6*, 1533.

[33] C. Zou, C. Amaya, S. Fasold, A. A. Muravsky, A. A. Murauski, T. Pertsch, I. Staude, *ACS Photonics* **2021**, *8*, 1775.

[34] R. E. Yardley, E. R. Gillies, *J. Polym. Sci., Part A: Polym. Chem.* **2018**, *56*, 1868.

[35] T. Wang, Y. Yu, D. Chen, S. Wang, X. Zhang, Y. Li, J. Zhang, Y. Fu, *Nanoscale* **2017**, *9*, 1925.

[36] S. Cormier, T. Ding, V. Turek, J. J. Baumberg, *Adv. Opt. Mater.* **2018**, *6*, 1800208.

[37] F. D. Jochum, P. Theato, *Chem. Soc. Rev.* **2013**, *42*, 7468.

[38] D. Roy, J. N. Cambre, B. S. Sumerlin, *Prog. Polym. Sci.* **2010**, *35*, 278.

[39] M. A. Stuart, W. T. Huck, J. Genzer, M. Muller, C. Ober, M. Stamm, G. B. Sukhorukov, I. Szleifer, V. V. Tsukruk, M. Urban, F. Winnik, S. Zauscher, I. Luzinov, S. Minko, *Nat. Mater.* **2010**, *9*, 101.

[40] M. Wei, Y. Gao, X. Li, M. J. Serpe, *Polym. Chem.* **2017**, *8*, 127.

[41] G. Kocak, C. Tuncer, V. Bütün, *Polym. Chem.* **2017**, *8*, 144.

[42] J. Thevenot, H. Oliveira, O. Sandre, S. Lecommandoux, *Chem. Soc. Rev.* **2013**, *42*, 7099.

[43] F. Diehl, S. Hageneder, S. Fossati, S. K. Auer, J. Dostalek, U. Jonas, *Chem. Soc. Rev.* **2022**.

[44] O. Grimm, S. C. Maßmann, F. H. Schacher, *Polym. Chem.* **2019**, *10*, 2674.

[45] O. Grimm, F. H. Schacher, *Polymers* **2018**, *10*, 645.

[46] D. Roy, W. L. Brooks, B. S. Sumerlin, *Chem. Soc. Rev.* **2013**, *42*, 7214.

[47] J. Seuring, S. Agarwal, *Macromol. Rapid Commun.* **2012**, *33*, 1898.

[48] A. Halperin, M. Kroger, F. M. Winnik, *Angew. Chem., Int. Ed.* **2015**, *54*, 15342.

[49] M. Glassner, M. Vergaelen, R. Hoogenboom, *Polym. Int.* **2018**, *67*, 32.

[50] R. Hoogenboom, H. Schlaad, *Polym. Chem.* **2017**, *8*, 24.

[51] G. G. Hedir, M. C. Arno, M. Langlais, J. T. Husband, R. K. O'Reilly, A. P. Dove, *Angew. Chem., Int. Ed.* **2017**, *56*, 9178.

[52] G. Vancoillie, D. Frank, R. Hoogenboom, *Prog. Polym. Sci.* **2014**, *39*, 1074.

[53] S. De Martino, F. Mauro, P. A. Netti, *Riv. Nuovo Cimento* **2021**, *43*, 599.

[54] J. Zhang, H. Tian, *Adv. Opt. Mater.* **2018**, *6*, 1701278.

[55] Y. Zhuang, X. Ren, X. Che, S. Liu, W. Huang, Q. Zhao, *Adv. Photonics* **2020**, *3*, 014001.

[56] J. Wang, Y. Zheng, L. Li, E. Liu, C. Zong, J. Zhao, J. Xie, F. Xu, T. A. F. König, M. G. Saphiannikova, Y. Cao, A. Fery, C. Lu, *ACS Appl. Mater. Interfaces* **2019**, *11*, 25595.

[57] A. S. Kupriianov, Y. Xu, A. Sayanskiy, V. Dmitriev, Y. S. Kivshar, V. R. Tuz, *Phys. Rev. Appl.* **2019**, *12*, 014024.

[58] K. Koshelev, A. Bogdanov, Y. Kivshar, *Sci. Bull.* **2019**, *64*, 836.

[59] S. Lepeshov, Y. Kivshar, *ACS Photonics* **2018**, *5*, 2888.

[60] A. S. Brar, M. Thiyagarajan, *Polymer* **1998**, *39*, 5923.

[61] Y. Liu, K. Sakurai, *Chem. Lett.* **2017**, *46*, 495.

[62] W. Wang, K. Troll, G. Kaune, E. Metwalli, M. Ruderer, K. Skrabania, A. Laschewsky, S. V. Roth, C. M. Papadakis, P. Müller-Buschbaum, *Macromolecules* **2008**, *41*, 3209.

[63] D. Magerl, M. Philipp, X.-P. Qiu, F. M. Winnik, P. Müller-Buschbaum, *Macromolecules* **2015**, *48*, 3104.

[64] R. Kaissner, J. Li, W. Lu, X. Li, F. Neubrech, J. Wang, N. Liu, *Sci. Adv.* **2021**, *7*, eabd9450.

[65] J. Karst, M. Floess, M. Ubl, C. Dingler, C. Malacrida, T. Steinle, S. Ludwigs, M. Hentschel, H. Giessen, *Science* **2021**, *374*, 612.

[66] P. Poudel, S. Chandran, S. Majumder, G. Reiter, *Macromol. Chem. Phys.* **2018**, *219*, 1700315.

[67] T. Shimoboji, Z. L. Ding, P. S. Stayton, A. S. Hoffman, *Bioconjugate Chem.* **2002**, *13*, 915.